ARA Information

Issue 1 ■ Fall 2022

Also in this issue:

Office Address:
No. 401, 4th Floor, No. 1 Bldg, Bay Square, Business Bay.
P.O.Box: 39337, Dubai – U.A.E.

Showroom & Training Center:
Flat 929, Tamani Arts Offices Building
Al Asayel St., Business Bay Dubai, U.A.E.

+971 (0) 4 4515339 | +971 (0) 50 378 8520

+971 (0) 4 4516309

www.ara.ae **info@ara.ae**

ARA
INFORMATION
Issue 1 ■ Fall 2022

Contents

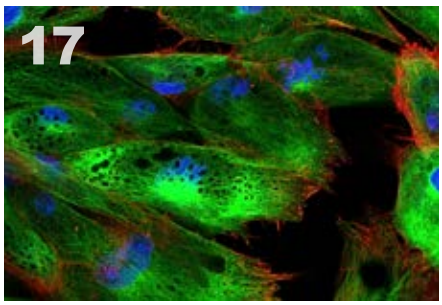

Welcome

Alireza Hedayatpour
Managing Director
ARA Spectron
Scientific & Laboratory
Equipment Trading L.L.C

WE ARE TRULY THRILLED AND HONORED to publish the first edition of our magazine, ARA Information, with the aim of introducing novel and innovative ideas and the latest technologies developed by leading scientists to aid the industries to meet today's challenge of transitioning to "nature-friendly industries".

Enjoying a team of experienced experts and esteemed international partners in preserving species and natural resources for future generations prompted us to publish this quarterly magazine.

We aim to contribute to the publication of the knowledge accumulated by accredited scientists and innovative methods and analytical instruments developed by knowledge-based companies.

The articles in each edition of ARA Information have been divided into the three chapters below:

1.Quality control of products: This chapter concern mostly laboratory testing for quality control of the products with those tests monitor the quality of products during the production process and in some finished products. Most of these tests are performed in the laboratory, and generally follow the methods provided by the respective and worldwide recognized Standard Organizations.

2.Know-How: in this chapter, we focused on a set of skills necessary for good performance in the Laboratory. These articles discuss the major lab skills that a chemist should have, as well as some tips on how to improve them. We would like to share knowledge on Laboratory Practices, Experimental Skills, Proper Handling of Laboratory Equipment, Analytical Methods, scientific writing and record-keeping, and problem-solving skills.

3.Environment Protection: In this chapter, we share the latest technology to pave the grounds for developing clean industries and reducing human pollution in the current critical conditions.

If you would like to learn about how we do this, please visit our new magazine.

The first edition of ARA Information is focused on the most polluting Industries; Oil, Gas, and Petrochemicals.

Undoubtedly, today's human development is in great debt with the breakthroughs and accomplishments in oil, gas, and petrochemical industries over the past two hundred years. Meanwhile, the misuse of these achievements has brought us to the brink of destroying nearly all biological resources which have caused the alarm for the crisis of not having access to healthy natural resources for all humans to be heard louder than ever before.

Through appreciating the magnitude of the current menace and acknowledging that overcoming this crisis depends upon individual development, we sincerely hope that we the humans, shoulder to shoulder with the world leaders like the ones in The United Arab Emirates, will make a unanimous global effort to avert the current major threat by relying on education and knowledge exchange.

Please join us on this journey and discover sustainable solutions for today's and tomorrow's world

Salute to green forest, blue skies, smile of the buds, and shining days!

Houshang Noorizadeh
PhD in Analytical Chemistry
Chromatography Product Manager

Determination of Aromatic Hydrocarbon Types in Middle Distillates Based on IP391/ASTM D 6591

Introduction:

This Test Method covers a high performance liquid chromatographic test method for the determination of monoaromatic, di-aromatic, and polyaromatic hydrocarbon contents in diesel fuels and petroleum distillates boiling in the range from 150 to °400C. The total aromatic content in % m/m is calculated from the sum of the individual aromatic hydrocarbon types.

This test method is calibrated for distillates containing from 4 to 40 % (m/m) mono-aromatic hydrocarbons, 0 to 20 % (m/m) di-aromatic hydrocarbons, 0 to 6 % (m/m) polycyclic aromatic hydrocarbons, and 4 to 65 % (m/m) total aromatic hydrocarbons.

Determining the aromatic content of hydrocarbon fuels is crucial to assessing their combustion characteristics and compliance with environmental regulations.

Two methods that are used for quantitation of aromatic components of fuels are ASTM D6379 and D6591, for kerosene and middle distillates (e.g., jet fuel) and diesel fuel, respectively. These methods are normal-phase, liquid chromatography methods in heptane mobile phase that separate and quantitate aromatics from fuel samples by refractive index detection.

It is important to ascertain the total level of aromatic hydrocarbon types in motor diesel fuel as it is a factor that can affect exhaust emissions and fuel combustion characteristics, as measured by cetane number. Due to limits on total aromatics content and polynuclear aromatic hydrocarbon content of motor diesel fuel by environmental regulation agencies, it is required to show compliance with appropriate analytical determination.

To ensure that the finished fuel products are safe and compliant, the aromatic hydrocarbon content level must be assessed by the ASTM D6591 test method and meet the criteria within.

Experimental:

A known mass of sample is diluted in the mobile phase, and a fixed volume of this solution is injected into a high performance liquid chromatograph, fitted with a polar column.

Apparatus:

High Performance Liquid Chromatograph (HPLC), Sample Injection System, Column System Any stainless steel HPLC column(s) packed with an approved amino-bonded (or polar amino/ cyano-bonded) silica stationary phase6 is suitable, Column lengths from 150 to 300 mm with an internal diameter from 4 to 5 mm and packed with 3 or 5 µm particle size stationary phase have been found to be satisfactory.

HPLC Column Oven, Backflush Valve, Refractive Index Detector, Computer or Computing Integrator.

Sample:	Diesel fuel, Engine oil, …
Sample Preparation:	Used sample after filtration
System	Normal phase
Eluent:	n-Heptane
Flow:	1.0 ml/min
Injection Volume:	10 µL
Temperature:	25 ˚C

Results:

After set the instrument parameters and equilibrate the system, the sample and standard was injected to the column and switch the back flushing valve at 8 min after injection.

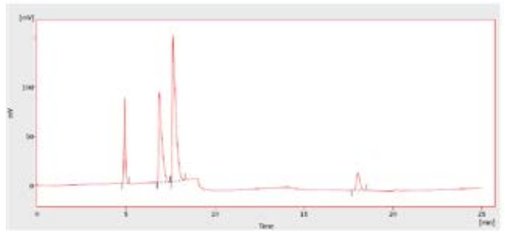

Fig.1: chromatogram of NA, MAH, DAH and TRI+

Fig.1 shows the chromatogram of NA (None Aromatic), MAH, DAH and TRI+ compounds and table 2 demonstrate the chromatogram results.

Component	Area	Height	Concentration	Units
None Aromatic	493.525	87.513	0.5	%w/v
MAH	1118.213	91.324	0.25	%w/v
DAH	1888.224	148.564	0.25	%w/v
TRI+	238.387	17.847	0.05	%w/v

Table 2: results of NA, MAH, DAH and TRI+ chromatogram

The calibration cure for each component based on concentration in table 3 was plotted and shows the relation between concentration of Cyclohexane, O-Xylene, -1Methylnaphthalene and Phenanthrene as standard components and NA (None Aromatic), MAH, DAH and TRI+ as aromatic hydrocarbon types in middle distillates.

Calibration Standard	Cyclohexane g/100 mL	O-Xylene g/100 mL	-1Methylnaphthalene g/100mL	Phenanthrene g/100mL
A	5	4	4	4
B	2	1	1	2
C	0.5	0.25	0.25	0.05
D	0.1	0.05	0.02	0.01

Table 3: Concentrations of Calibration Components

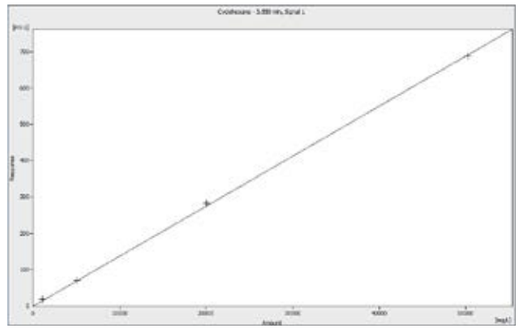

None Aromatic

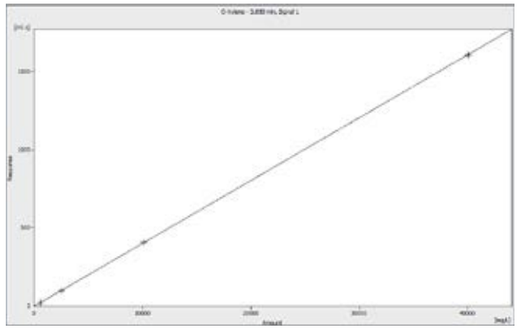

MAH

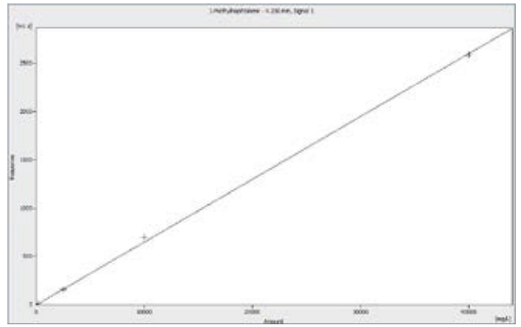

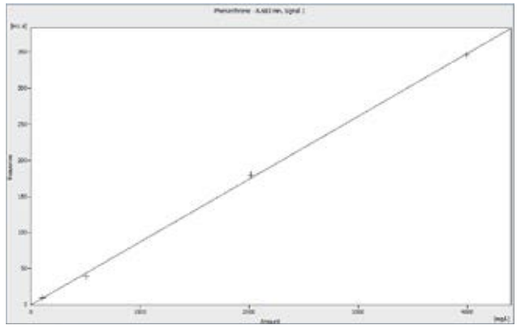

Reference:

[1] ASTM D 6591: Standard Test Method for Determination of Aromatic Hydrocarbon Types in Middle Distillates—High Performance Liquid Chromatography Method with Refractive Index Detection
[2] ASTM D 1319 Test Method for Hydrocarbon Types in Liquid Petroleum Products by Fluorescent Indicator Adsorption.
[3] IP Standard Test Method for Determination of Aromatic Hydrocarbon Types in Middle Distillates – High Performance Liquid Chromatography Method with Refractive Index Detection.
[4] D 2425 Test Method for Hydrocarbon Types in Middle Distillates by Mass Spectrometry.

Dr. Mehdi Asgari
PhD in Analytical Chemistry
Technical Manager

WATER SEPARATION Characteristics of Aviation Turbine Fuels

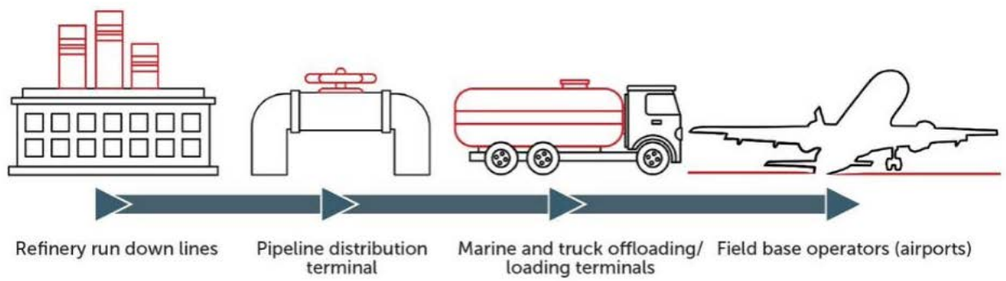

Introduction:

The Increased Effort for renewable energy sources has promoted a variation of alternative energy sources introduced into industry.

An essential consideration in the manufacturing jet fuels is their composition as well as how this composition changes with the processing both during manufacturing and transportation before operation.

The water separability tests are necessary to the proper characterization of jet fuels as even the smallest change to fuel composition can affect the performance of filter-separator equipment. Therefore, fuel purification efficiency is reduced by fuel additives and even trace amounts of surfactants. If even a small amount of water is to pass through filtration above an additive allowable threshold, it can freeze inside the fuel system of an aircraft potentially causing serious damage to it.

The WSI (Water Separation Index) was developed in conjunction with industry stakeholders to measure for the presence of surfactants rapidly and precisely in jet fuel. The instrument was designed to be user-friendly with a minimum of training and its powerful design makes it expedient for field laboratories. ASTM and EI test methods have been developed and now they are approved for use in accordance with ASTM D1655 Appendix XI and JIG Bulletin 121.

The Joint Inspection Group (JIG), published their Product Quality Bulletin number 121 which revises the Protocol for Water Separation Testing Downstream of Point of Manufacture and advises testing can be done using ASTM D8073 (IP 624).

After that, JIG has issued bulletin 142 recommending the use of ASTM D8073, WSI for Water Separation Testing.

JIG is responsible for protecting and updating the Aviation Fuel Quality Requirements for Jointly Operated Systems (AFQRJOS) as well as known as “checklist”.

The latest bulletin 142 provides the industry with an update on the work engaged, looking in accordance with ASTM test methods for determining the water separation properties of JET Fuel.

JIG has revised the Protocol for Water Separation

Testing Downstream in Manufacturing and now advise testing using ASTM D8073.

JIG has stated 'As this method has not shown the same variability of other methods, it has been identified as the preferred method for water separation testing for fuels containing Static Dissipater Additive.

Principles of Operation:

Before each test the Water Separation Instrument rinse the test sample, prepare the instrument and prepare the filter. When the test starts the unit pumps added water into the test sample and emulsifies the solution with an ultra-sonicate. After a defined time, the emulsion is pumped through a particulate filter, the detector and into the waste container to provide a reference value. Once a reference value is gained, the emulsion is diverted through a filter cartridge to remove the added water before it passes through the detector again and a new set of readings are taken. The water separation index is calculated from the reference value and subsequent readings. Results display on the screen.

Results are calculated from the detector reading and displayed on screen as the WSI. A high WSI, such as 100, indicates the sample coalesces easily and is relatively free of surfactants.

Reference:

[1] bulletin NO. 142; testing water separation properties of jet fuel; JIG; 07/04/2022.

[2] Stanhope Seta News, https://www.stanhope-seta.co.uk/2022/05/06/jig-142-product-quality-bulletin-issued-astm-d8073-preferred-test-method/; 6TH MAY 2022

Houshang Noorizadeh

PhD in Analytical Chemistry

Chromatography Product Manager

Critical Points in Determination of Aromatic Hydrocarbon by NP HPLC

There are the determination of aromatic that may cause failure in resolution achievement. Based on ASTM D6591, the resolution should be more than 5 for mono and di aromatic hydrocarbons.

It recommends any stainless steel HPLC column(s) packed with an approved amino-bonded (or polar amino/cyano-bonded) silica stationary phase. But experiences show it couldn't have achieved good resolution with some amino-bonded columns. Then mono, di, and polynuclear aromatic do not separate properly. So it is very important to choose a column with suitable properties.

Amino columns contain a silica-based aminopropyl bonded sorbent. The column is listed as USP L8 and is used for normal-phase separations. Some properties of this column is:

Base Material: Silica, **Functional Group:** aminopropyl, **Particle Size (µm):** 3, **Carbon Load (%):** >%2, **Endcapped:** No

Silanol Activity: High, **Pore Size:** 80 ºA,**Column Size (mm) I.D. × Length**: 250 × 4.6,**Particle Shape:** Spherical

The Spherisorb Amino (NH2) Column from Waters company is good example for these type of columns.

The second point is mobile phase purity. Normal phase chromatography is very sensitive to polar solvent and resolution decreases with polar solvent impurities (like methanol and water). So there is a need to equilibrate the column with high purity nonpolar solvent (such as n-heptane).

The conditioning of the column is between 3 h and two days based on the situation. Using another solvent for solving polar impurities sometimes increases the speed and efficiency of equilibration.

In addition, check valves are suffering from loss of performance because of using the nonpolar solvent with a low boiling point. There is friction between piston and piston gasket (or piston seal). So the pump head becomes warm and the solvent could not transfer the heat. It increases the friction because of interaction with the piston gasket. So using active back flushing for washing pistons or using the cooling system for the head pump could help.

Farid Sheikh-Hasani
MSc of polymer chemistry
Particle & Polymer Testing Product Manager

Particle Size Determination

Hard to Disperse Samples:

a) Static charge respectively also hydrophobic characteristics

b) Adhesive powers

It is **A**lways astounding that the market for highly precise, fully automatic analytical instruments is permanently growing, while no emphasis is placed on the equally important sample preparation or sampling. One of the most common mistakes during analysis is already made during the sampling stage and drawn into the analytical procedure right from the beginning.

Fist step is sample division, The sample for the Laser Particle Sizer ANALYSETTE 22 shall correspond in the contained particle type and particle distribution with the entire batch of material. The Rotary Cone Sample Divider LABORETTE 27 is very well suited for the division of dry laboratory samples or suspensions, since different dividing heads with different division ratios can be selected. Depending on the division head up to 3000 dividing steps per minute can be achieved.

Next step is Sample dispersion, Via pre-tests it must determined in which manner the sample material can be moistened and dispersed. The liquid should possibly completely and spontaneously wet the solid matter. The additional ultrasonic support (if possible with maximum power) in general reduces the dispersion duration.

Unproblematic samples, which submerge without any great effort directly into the surface of the water and possess no large amount of fine share, are added to the dispersion unit as a solid material with a spatula portion by portion and after a brief ultrasonic treatment/ dispersion (60-30s) measured reproducibly.

Samples hard to disperse may display the following characteristics: static charge (for example plastics), adhesive forces or cohesive powers – samples tend to conglutinate/ agglutinate – (for example clays, soil samples, kaoline), magnetism, hydrophobic characteristics – water repellent molecule components (for example drugs, medications, toner, graphite, titanium dioxide, waxes), coagulation (for example clays, kaoline, chalk, gypsum).

a) Static charge respectively also hydrophobic characteristics

Here a spatula amount of the material should be added to a small Erlenmeyer flask and then at first a few drops of a wetting agent (surfactant or diluted surfactant solution) added, then mixed into a paste until the sample is completely wetted. Water is added

drop by drop and stirred. The now created suspension is dispersed in an ultrasonic bath. If the sample is already inside the dispersion unit and floats on top of the surface, the sample can be wetted as follows: With a glass rod or with the tip of a spatula, a small drop of the wetting agent is added/touched on the surface of the liquid and distributed. Immediately it can be seen, that the formed skin on the surface breaks open and the fine portion enters the suspension.

b) Adhesive powers

are clinging powers of the particle. A reduction of these surface powers can be obtained by creating on the boundary phase areas from solid/ liquid, adsorption layers from surface-active agents or macromolecules. It is considered a covering, a guarding or masking of the solid material respectively wetting. For this reason in most cases for example tetra-Na-diphosphat or poly sodium are utilized.

Mitra Amoli Diva
PhD in Analytical Chemistry
Spectroscopy Application Manager

How Does a Spectrometer Work?

Over the past years, miniature fiber optic spectrometers have evolved from a novelty to the spectrometer of choice for many modern spectroscopists. Researchers found the advanced utility and flexibility provided by their small size and compatibility with a huge amount of sampling accessories.

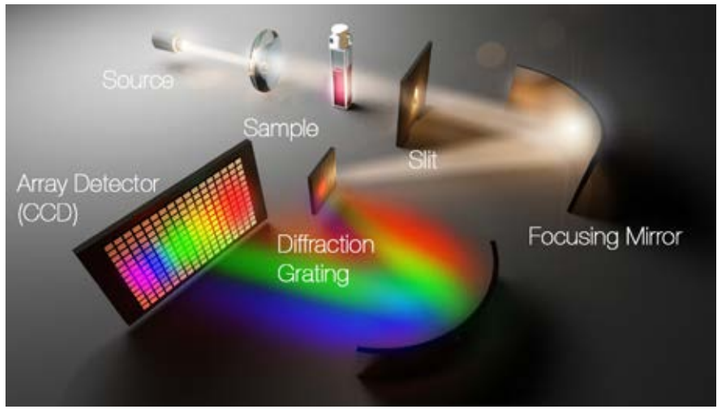

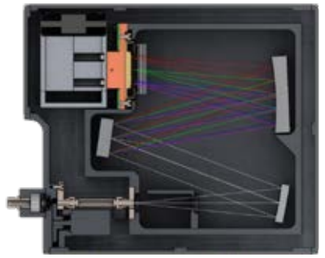

The entrance slit:

The slit determines the amount of light (photon flux) that enters the optical bench and is essential for the performance of spectrometers. It is also a driving force in the determination of spectral resolution. Other factors are groove frequency, detector pixel size, and grating.

The angle of the light that enters the optical bench is controlled by the slit. Slit widths are available in several different sizes from 5 µm to as big as 800 µm with a 1 mm (standard) to 2 mm height. As slits are aligned and permanently mounted into a spectrometer and should only be changed by a trained technician, it is essential to choose the appropriate slit for an application.

Technical Details:

The function of the entrance slit is to define a clear-cut object for the optical bench. One of the key factors that it impacts the throughput of the spectrometer is the size (height (H_s) and width (W_s)). The image width of the entrance slit is an important factor in finding the spectral resolution of the spectrometer when it is greater than the pixel width of the detector array. An appropriate entrance slit width should be selected to balance the resolution and throughput of a system.

The image width of the entrance slit (W_i) can be estimated as:

$Wi = (M^2 \times W_s^2 + W_o 2)^{1/2}$

Where M is the magnification of the optical bench that is set by the ratio of the focal length of the focusing mirror (lens) to the collimating mirror (lens); W_o is the image broadening caused by the optical bench; and Ws is the width of the entrance slit. W_o is on the order of a few tens of µm for a CZ optical bench.

So, reducing the width of the entrance slit below this value will not significantly improve the resolution of the system. The axial transmissive optical bench offers a considerably smaller Wo and so can achieve a considerably higher spectral resolution. The pixel width (W_p) of the array detector sets another limit on spectral resolution. Reducing Wi below Wp will not help increase the resolution of the spectrometer. If the resolution requirement is satisfied, the slit width should be as wide as possible to enhance the throughput of the spectrometer.

The Grating:

The diffraction grating of a spectrometer partially determines the optical resolution that can be achieved by the spectrometer and also determines the wavelength range. Selecting the correct grating is an important factor to optimize a spectrometer to obtain the best spectral results for the application. There are two parts in the grating, the blaze angle and groove frequency, both of which are explained in detail in the following sections.

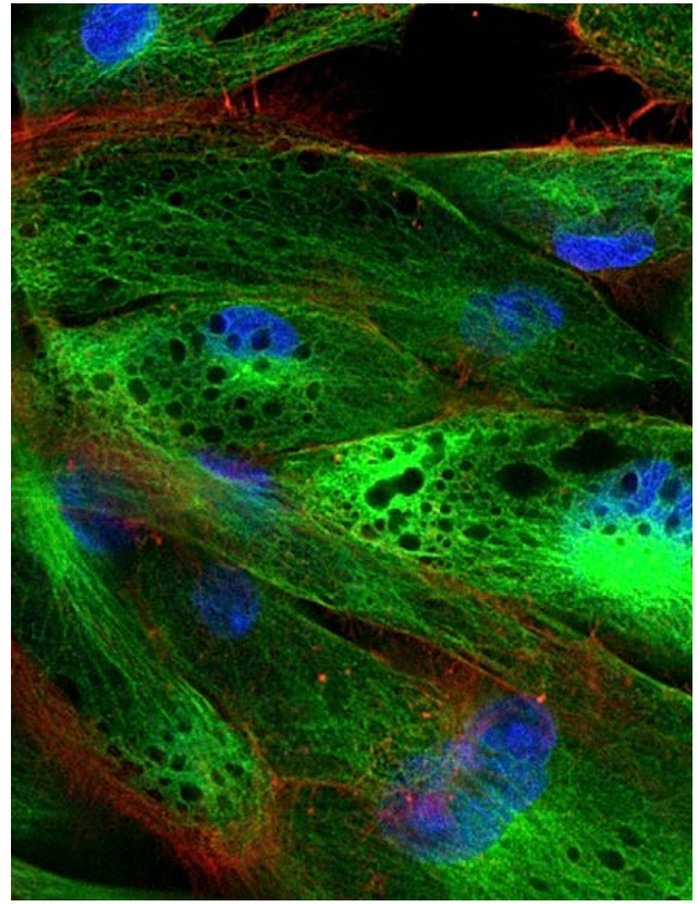

There are two types of diffraction gratings – holographic gratings and ruled gratings. Ruled gratings are developed by etching several parallel grooves onto the surface of a substrate and then coating it with a highly reflective material.

Holographic gratings are developed by interfering two UV beams to create a sinusoidal index of refraction variation in a piece of optical glass. This technique provides a more uniform spectral response, but a considerably lower overall efficiency.

Groove Frequency:

The amount of grooves per mm ruled into the grating determines the amount of dispersion. This is commonly known as groove frequency or groove density. The spectrometer's wavelength coverage is determined by the groove frequency of the grating, which is also a key factor in the spectral resolution.

Optical signals in wavelengths from different diffraction orders may end up at the same spatial position on the detector plane when the required wavelength coverage is broad, i.e. λmax > 2λmin.

Blaze Angle:

As a grating diffracts incident polychromatic light, it doesn't do so with uniform efficiency. The groove facet angle, also known as the blaze angle, determines the overall shape of the diffraction curve. With this property, it is possible to calculate which blaze angle will correspond to which peak efficiency; this is known as the blaze wavelength. Figure 2 illustrates this concept and compares three different 150 g/mm gratings blazed at 500 nm, 1250 nm, and 2000 nm.

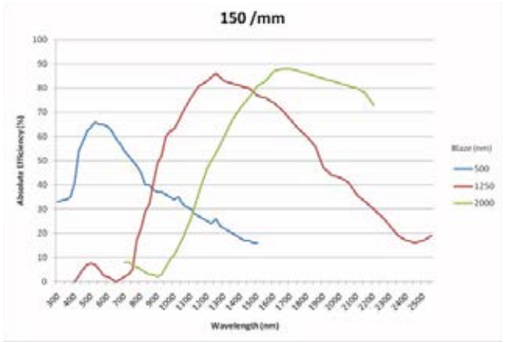

Gratings can be blazed to provide high diffraction efficiency (>%85) at a specific wavelength, i.e. a blaze wavelength (λB). As a rule of thumb, the grating efficiency will decrease by %50 at 0.6 xλB and 1.8 xλB. This sets a limit on the spectral coverage of the spectrometer. Typically, to improve the overall signal to noise ratio (SNR) of the spectrometer, the blaze wavelength of the diffraction grating is biased toward the weak side of the spectral range.

The Detector:

In traditional spectrometer (monochrometer) designs, a second slit is located in the image plane, called the exit slit. Usually, this exit slit the same size as the entrance slit, given that the width of the entrance slit is one of the limiting factors on the spectrometer's resolution.

In this configuration, an element detector is positioned behind the exit slit and this is followed by rotating the grating to scan the spectral image across the slit. Thus, the intensity of the light is measured as a function of wavelength.

In modern spectrometers, linear detector and CCD arrays have enabled the development of "fixed grating" spectrometers. When the pixels across the CCD are hit by the incident light, each pixel represents a part of the spectrum that the electronics can translate and display with a given intensity using software.

This development has made it possible to construct spectrometers without any moving parts, considerably reducing the size and power consumption. Compact multi-element detectors have enabled the development of a new class of low-cost, compact spectrometers that are generally known as "miniature spectrometers."

Detector Types:

Although there are different ways to characterize photodetectors, the most significant differentiator is the detector material. Si and InGaAs are the two most common semiconductor materials employed in miniature spectrometers.

When designing a spectrometer, it is important to choose the right detector material because the upper wavelength limit (λ_{max}) is detected by the bandgap energy (Egap) of the semiconductor. λmax can be detected by the relationship given below:

$\lambda max = hc/E_{gap}$

Where, c is the speed of light and h is Plank's constant. The speed of light and the product of Plank's constant can be expressed as 1.24 eV•μm or 1240 eV•nm to simplify the conversion of energy into wavelength. For instance, Si's bandgap energy is 1.11 eV which corresponds to the maximum wavelength of 1117.117 nm.

On the other hand, InGaAs is an alloy formed by mixing InAs and GaAs, which have respective bandgap energies of 0.36 eV and 1.43 eV. The bandgap energy, based on In and Ga ratios, can be tuned in between those two values. It is slightly harder to quantify the lower detection limit of a material, because it is determined by the absorbance characteristics of the semiconductor material, and can differ widely with the detector thickness.

The detection limit of the detector can also be lowered by placing a fluorescent coating on the window of the detector, which will then absorb the higher energy photons and reemit lower energy photons, which are subsequently detected by the sensor. A comparison of the detectivity (D*) as a function of wavelength for both InGaAs and Si (CCD), is shown in Figure 1.

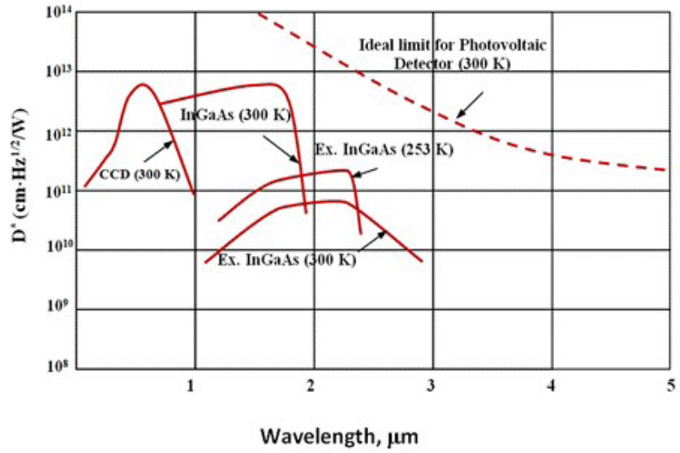

Figure 1. Approximate D values as a function of wavelength for some typical detectors*

CCDs, BT-CCDs, and PDAs:

Currently, InGaAs detector arrays are only available in one configuration, but Si multi-element detectors are available in three different subcategories - back-thinned charge coupled devices (BT-CCDs), charge coupled devices (CCDs), and photodiode arrays (PDAs).

CCD technology enables the construction of small pixel size (~14 μm) detectors as it removes the requirement of direct readout circuitry from individual pixels. To achieve this, the charge is transferred from one pixel to another, enabling all of the information along the array to be read out from one pixel.

CCDs are an ideal option for most miniature spectrometers, as they can be designed quite inexpensively. However, they come with two disadvantages; first, the gate structure located on the front of the CCD can make the incident light scatter, which means it won't be absorbed, and second, a relatively large P-Si substrate is required by CCDs to ease low cost production, but this also limits the detector's efficiency (particularly at shorter wavelengths) as a result of absorption through the Player.

BT-CCDs provide the ideal option to mitigate these problems in spectroscopy applications where very high sensitivity is required. BT-CCDs are designed by etching the CCD's P-Si substrate to a thickness of about 10 μm. This process not only reduces the amount of absorption, but also increases the detector's overall efficiency.

In addition, the detector is also illuminated from the back side (P-Si region), removing the effects from the gate structure on the detector surface. Figure 2 depicts a typical comparison of the quantum efficiency between a back-illuminated BT-CCD and a traditional front-illuminated CCD.

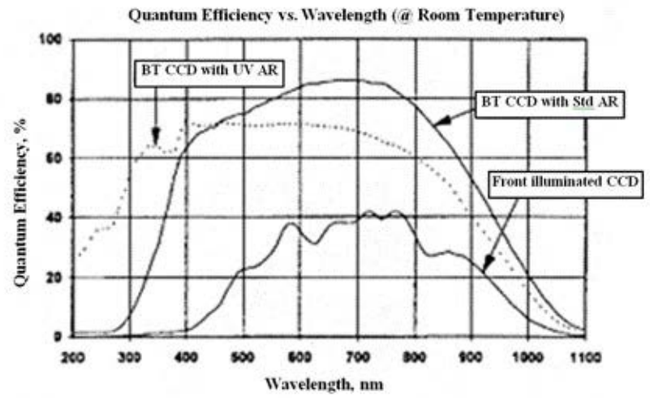

Figure 2. Typical quantum efficiency of front-illuminated CCD and back-illuminated CCD

While the use of BT-CCDs in spectroscopy provides clear benefits, there are two key drawbacks that should be taken into account. First, this process considerably increases the production cost, and second (as the detector is very thin) an etaloning effect can be caused by reflections off the front and back surfaces of the detector.

Although the etaloning effect associated with BT-CCDs can be mitigated by a deep depletion process, this will again increase the cost of the production process.

PDA detectors are more conventional linear detectors that contain a set of individual photodiodes arranged in a linear fashion using CMOS technology. While PDA detectors lack high sensitivity and small pixel size, they provide several benefits compared to BT-CCD and CCD detectors.

First, the absence of charge transfer removes the requirement for a gate structure on the front surface of the detector, and considerably increases the readout speed. Second, the well depth of a PDA detector is relatively higher than the well depth of a CCD - the well depth of a typical PDA detector is ~156,000,000e- compared to ~65,000e- for a typical CCD.

Due to the larger well depth, PDA detectors have an extremely linear response and a very large dynamic range ~50,000:1. These properties make these detectors suitable for applications where small changes in large signals, such as LED monitoring need to be detected.

The Optical Bench

Finally, the Optical Bench will determine how these components operate together with different optical components to create a complete system. Generally, this system is called the optical bench, or spectrometer.

Although many different possible optical bench configurations are available, the most common types are the crossed Czerny-Turner, unfolded Czerny-Turner, and concave holographic spectrometers.

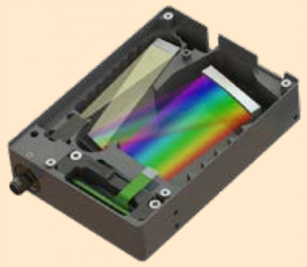

Reference:

[1] www.oceaninsight.com
[2] www.bwtek.com
[3] Portable Spectroscopy and Spectrometry, Applications Richard A. Crocombe, Pauline E. Leary, Brooke W. Kammrath, 2021
[4] Handbook of Spectroscopy, G. Gauglitz, T. Vo-Dinh, 2006

Dr. Mehdi Asgari
PhD in Analytical Chemistry
Technical Manager

Heavy Metal Analysis
in Water using the Screen-Printed Electrodes

Introduction:

HEAVY METALS (HMSs) are important sources of hazardous contaminants in ecological systems. They cause potential and serious problems in aquatic organisms and people. Studies on heavy metals in aquatic eco ecological systems can provide valuable information about the environmental condition of that ecosystem. The water and sediment of the polluted sites contain different levels of heavy metals. Measurement of heavy metals in both water and sediment samples can show the condition of the ecosystem with respect to heavy metal pollution. On the other hand, aquatic organisms are the target of heavy metal intoxication, which accumulates large volumes of heavy metals in their tissues. Therefore, the measurement of heavy metals in the aquatic organisms will be valuable and informative.

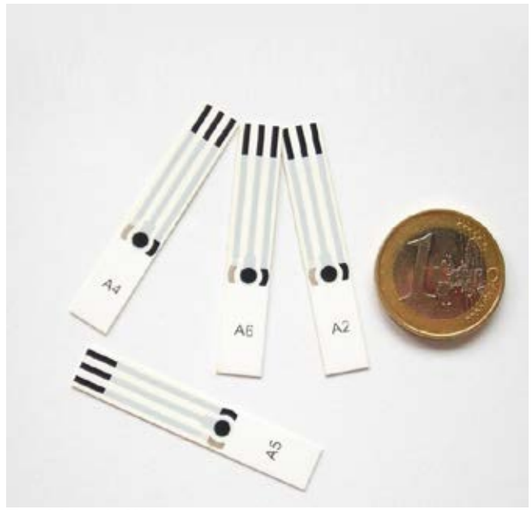

Figure 1. Schematic of SPE

Different heavy metals quantities are widely distributed in various environments with particularly high toxicity, which highlights the urgency for effective and rapid detection methods. Traditionally used analytical methods for the detection of HMS include Atomic Absorption Spectroscopy (AAS) and Inductively Coupled Plasma Mass Spectroscopy (ICP-MS). These Analytical techniques have advantages of high sensitivity and selectivity; however, they must be performed in a laboratory, which requires transportation of the samples to the laboratory, and they are expensive instruments and should be run by trained personnel.

On-site heavy metal determination in water, avoiding any pretreatment, and maintaining the most original characteristics of HMs, have shown the advantages compared to the traditional approaches for HMs distribution assessment in waters including sampling, laboratory measurement, and possible contamination. To further decrease the labor errors and cost from on-site HMs measurements, several automatic sensing probes based on anodic stripping voltammetry have been reported in the literature; however, they yet endure from the low portability caused by the big amount and lack of far operation and automation, requiring peoples on deck to control the movements of probes between different testing locations, which induces a high cost, especially in large lakes and rivers.

These days, electrochemical techniques are promising due to their portability, simplicity, and fast detection. Square-wave anodic stripping voltammetry (SWASV) is one of the most typical techniques for HMs detection.

This text aims to provide the user with a comprehensive set of instructions for use of the SPE in analyzing Pb, Cd and Cu concentrations of a polluted water sample.

Experimental:

This analysis will be performed utilizing SWV using PalmSens, EmStat or EmStat Blue with PSTrace software or PStouch with the parameters as described on reference [5].

Results:

This example is set for a typical river water sample, but concentrations of metals can vary massively from location to location. The electrodes do have a large linear range but if the electrode is saturating then the deposition time needs to be lowered.

Metal	LOD (ppb)	~Slope (nA/ppb)	Linear range (ppm)
Cu	<1	30	1-1000
Pb	<1	115	1-1000
Cd	<1	60	1-1000

*Table 2 the typical LOD for 120s deposition. Calculated using 3*standard deviation of repeat measurements of 1ppb of each metal*

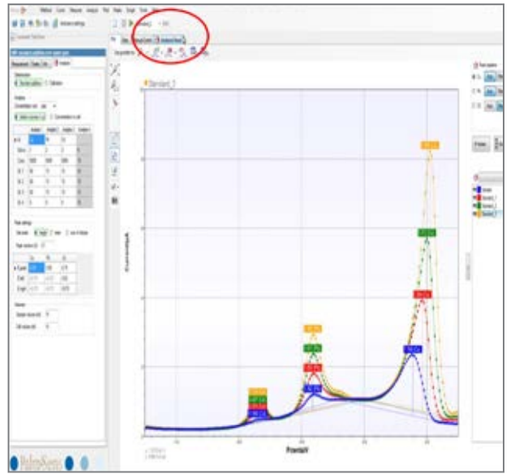

All the data (raw or calculated) can be exported or printed for further manipulation using the All to clipboard and the Print buttons at the top of the data screen (fig.2).

Figure 2.The final analytical scans and where to find the analytical results

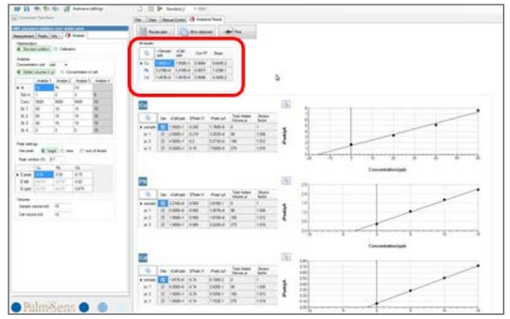

The electrode is sufficiently stable to calibrate in the morning, obtain the sensitivity (S) and use the same S for all measurements (concentration of metal in the sample = Ipeak/S).

Figure 2.The final analytical scans and where to find the analytical results

Reference:

[1] Jamshaid ,M.; Khan. A.A.; Ahmed. K. and Saleem M., Heavy metal in drinking water its effect on human health and its treatment techniques – a review International J. of Biosciences (IJB) 240–223 ,2018 , (4)12.
[2] Valavanidis, A. ; Vlachogianni, T.; Metal Pollution in Ecosystems: Ecotoxicology Studies and Risk Assessment in the Marine Environment. Science advances on Environment, Toxicology & Ecotoxicology issues, www.chem-tox-ecotox (2010).
[3] Palchetti, I.; Laschi, S.; Mascini, M.; Miniaturized stripping-based carbon modified sensor for in field analysis of heavy metals; Analytica Chimica Acta 67-61 ,2005 ,530.
[4] Smith, E.J.; Davison, W.; Hamilton-Taylor, J.; Methods for preparing synthetic freshwaters. Water Res.; 1296–1286 ;2002 ;36.
[5] Palmsens BV.; Detection-of-heavy-metals-IS-HMS08-12-2015-; December 2015 ,15.

Mitra Amoli Diva
PhD in Analytical Chemistry
Spectroscopy Application Manager

New Solutions of
Laser-Induced Fluorescence for Oil Pollution Monitoring at Sea

Laser-**i**nduced fluorescence (LIF) is an informative method to research a matter. Many scientists improve LIF to apply it for sea oil pollution monitoring. LIF application for oil spill monitoring at sea was studied for many years, but it still occurs. The competitive analysis of available sensors for oil pollution at sea shows that LIF is one of the most enlightening and informative methods for oil spill monitoring. It allows detecting the pollution and the recognition of the oil or oil products. The volume of the pollution by oil products (thin slicks on the sea surface or solutions in the seawater) may be evaluated based on the LIF spectra analysis.

Nowadays, there are quite distinctive LIF spectrometers for oil spill monitoring by plane or by vessel. In some cases, LIF spectrometers were used not only as scientific equipment but also to obtain the information about the exact pollution. However, the practice of using LIF spectra shows that airborne LIF spectrometers or its versions for the vessels may be beneficial only if it is applied for the specific research of big sea areas or offshore oil disasters. It is not efficient to use such equipment for everyday sea monitoring or oil spill monitoring at a regional scale. It is crucial to improve LIF application due to increased pollution which is caused by illegal bilge water disposal, bunkering accidents and other accidents of small scale. Such pollution at the regional scale is becoming a dominating part of the total pollution of the World Ocean.

LIF and necessary equipment have been developed in the recent years for commercial unmanned aerial vehicles (UAV). Laser technologies, methods, the equipment of spectral analysis and spectral data processing, including methods of artificial intelligence, are being improved. Now it is possible to start the development and design of the monitoring equipment which is beneficial, prompt and easy to be serviced for small scale pollution. This research is aimed to solve the following tasks for LIF:

- LIF development for the prompt measurement of concentrations of dissolved oil products in the seawater;
- Development of the identification method of oil product type, which caused the pollution (slick and dissolved state), by machine learning.

The first task is explained by a substantial volume of pollution, which is caused by illegal bilge water disposal by vessels. Pollution by bilge water is a process when oil products of different concentrations enter the upper layer of the ocean. This process does not always cause the slick on the sea surface, and it depends on the concentration value of the oil hydrocarbon in the bilge water and hydrology parameters of the marine environment. The permissible concentration for dissolved oil hydrocarbons is 15 ppm, limited for bilge water disposal by vessels. This concentration is quite a small, and this it is now essential to develop the prompt LIF method which can measure such small concentrations of oil hydrocarbons in the seawater.

The second aforementioned task may be solved within a broad scope of LIF. There are developed methods of identification for different types of oil products which are based on the analysis of distinct LIF spectra. These methods are based on the analysis of distinctive features of the LIF spectra (maxima position, the intensity ratio of the chosen spectral bands or time-resolved fluorescence). Nonetheless, recognition methods of oil types by LIF spectra may be improved by methods of recognition which are based on machine learning. It is therefore crucial to collect data sets with the LIF spectra of solutions and slicks of the most common types of marine fuels. It is necessary to research the LIF spectral characteristics of oil products in different states such as thin slick on the sea surface or solution in the seawater. Such distinctive features of spectra should be defined for each type of oil product which are often noticed as pollutants of the ocean. Machine learning must include all of these distinctive features to recognize different types of oil products.

This research presents laboratory investigations of LIF spectra which may widen the scope of LIF application for monitoring sea pollutions. The results of this research were used by the authors to develop essential elements of artificial intelligence which allow for classifying the LIF spectra of oil products. Moreover, we aimed to develop a small-sized LIF sensor which can be used by different carriers such as vessels, remotely operated vehicles and especially unmanned aerial vehicles.

Experimental Set-Up, Method and Materials:

The LIF spectral distributions for the different types of oil products and crude oil were investigated. The most widespread types of marine fuel were chosen; these types of fuel are common for polluted sea areas in the time of bunkering or bilge water disposal. DMZ, DMA (Distillate Marine fuels refer to categories Z and A, respectively), diesel fuel and kerosene were investigated as a type of light fuels; RMB 30, RME 180, RMG 380 (Residual Marine fuels refer to category B, E and, G, respectively) and crude oil were investigated as a type of heavy fuels.

A small sized sensor was developed to investigate the LIF spectra of solutions and slicks (Figure 1). It was designed to be used by a small sized UAV. The sensor was designed to be used in two ways: LIF spectra measurement from surface slick (nadir LIDAR sensing) and LIF spectra measurement of oil product solution in the on-land regime when the sensor was submersed into the water. In this research, the sensor was designed and based on LIF signal values, which were measured at the laboratory. Moreover, it was based on LIF usage experience for slick spectra registration from UAV by the authors. Additionally, a 278 nm wavelength with strong absorption in water was used.

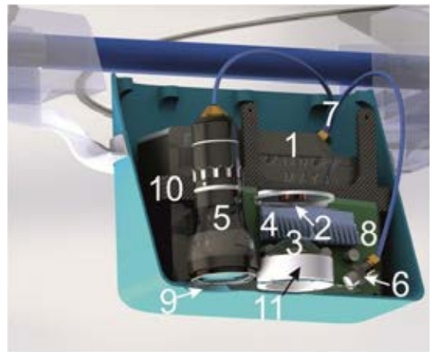

Figure 1: Smallsized laser-induced fluorescence (LIF) spectrometer. -1Maya 2000Pro spectrometer, -2laser diode 6060 UVS LED; -3collimator (quartz lens); -4radiator for LED; -5collimator (lens -84UV, this channel for LIDAR sounding); -84-6UV25- collimator (Ocean Optics); -7fiber-optic light guide P-2-600SR (Ocean Optics, this channel is open in the on-land regime, but closed in the LIDAR sounding); -8computer ITX-N;29 -9quartz port-light; -10holding of MAYA 2000Pro and computer; -11holding of lens.

The laboratory set-up in Figure 2 was used to investigate the LIF spectra of the solutions. The laboratory set-up included all the elements of a small sized LIF spectrometer. The sensor was 1 m above the cuvette when the slicks were measured at the laboratory. It was supposed in this research that such a height was appropriate when UAV was used to measure the LIF spectra from the oil slicks in situ.

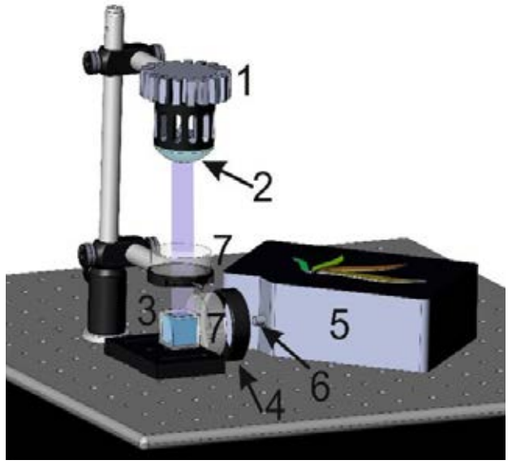

Figure 2. The laboratory set-up for the investigation of the LIF spectra of oil product solutions. -1radiator with LED; -2quartz lens; -3solution of oil product in the cuvette; -4filter (Newport 10CGA-5 ;(295-spectrometer Maya 2000Pro; -74-6UD collimator (Ocean Optics); -7quartz optical windows.

Firstly, the LIF spectra of the pure types of each oil product were measured to obtain etalons. There are distinctive distributions of the LIF spectra in Figure 3 for the different types of pure oil products which were discussed in the article, among which the heavy types of fuel are marked by dashed lines. The spectra were received by the radiation of the surface of the pure oil products volume in a back way (Figure 1). The left scale (Figure 3) is for the intensity of the light fuels including the DMZ, DMA, diesel fuel and the kerosene. The right one is for the heavier types of fuels such as RMB, RMG, RME and pure oil. The LIF spectral distributions were received in almost the same condition, and the values of the relative intensity (relative to the intensity at 295 nm) estimated the quantum efficiency of LIF for the different types of oil products. The values of the LIF intensities from the heavy types of fuels were smaller than the values from the light types, so we used 2 vertical axes to place these values in the linear scale. Subsequently, it was easy to note the distinctive differences of LIF spectra between the heavy and light types of fuel.

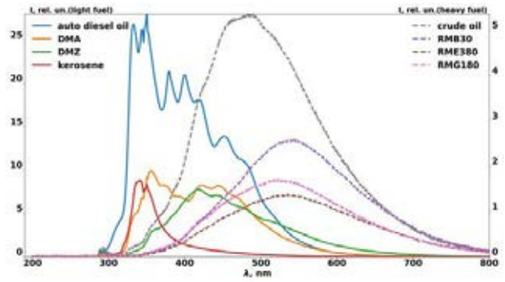

Figure 3. Oil product LIF spectra of the pure state.

The change of LIF spectra was investigated when the fuel state changed from the pure to the slick state, and then to the solution. The forms of the spectral LIF distributions are shown as an example depending on the state of the oil product for fuels in Figures 5-4. The LIF spectrum of the pure seawater and background radiation was measured before the spectra of the slicks and solutions were measured. The signals from the seawater fluorescence and background radiation were excluded from the summarized LIF signal.

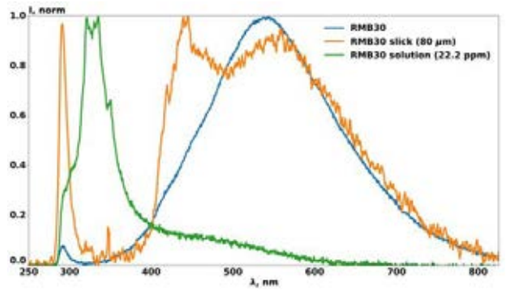

Figure 4. LIF spectra of the heavy RMB 30 marine fuel depending on its state.

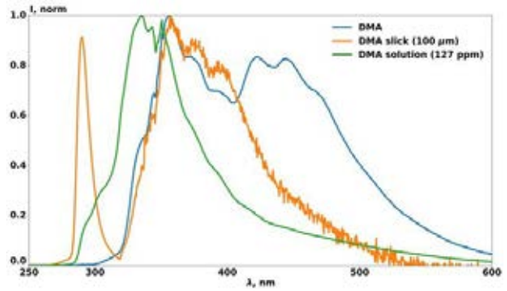

Figure 5. LIF spectra of the light DMA fuel depending on its state.

The LIF spectra from the solutions of DMA and RMB 30 in different concentrations in the seawater are shown in Figure 6 and Figure 7, respectively. The values of the concentrations of the solutions are shown in ppm. They correspond to the particular color of the diagram and are placed in the upper right part of the figures.

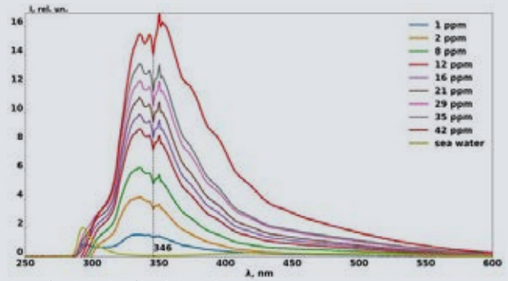

Figure 6. LIF spectra of the DMA solutions.

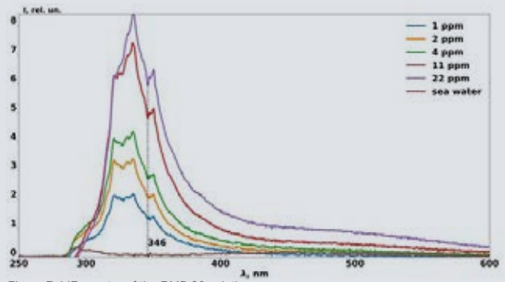

Figure 7. LIF spectra of the RMB 30 solutions.

The example of the LIF spectra data set, which was used for the machine learning of identification of the light type of fuel such as DMA is shown (Figure 8). The linear support vector classification (LinearSVC) algorithm was used to classify the spectra [33]. Five separate sequences of DMA fuel spectra are shown. Each sequence includes 30 spectra and corresponds to the exact concentration of oil products in the seawater.

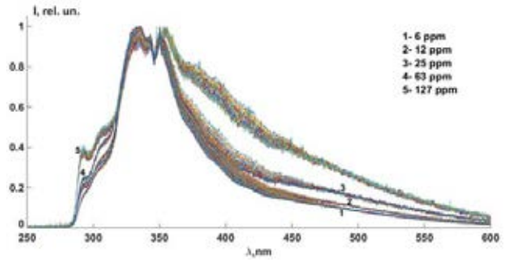

Figure 8. Sequences of the LIF spectra of the five concentrations of DMA solutions.

The sequence of crude oil solutions within the range of concentration 13-0.6 ppm is shown in Figure 9. The data sets of these examples represent extreme cases in machine learning for the identification of different types of oil products (light fuel and crude oil) in dissolved states in the surface layer at sea.

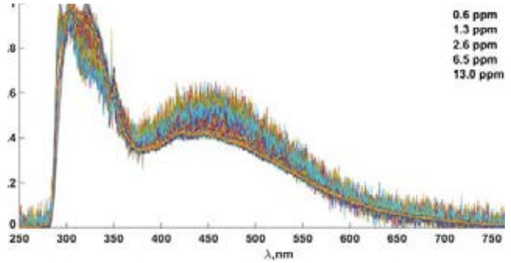

Figure 9. Sequences of the LIF spectra of the five concentrations of crude oil solutions.

The calibration function of the DMA solution is shown in Figure 10 as an example of the calibration of the LIF method.

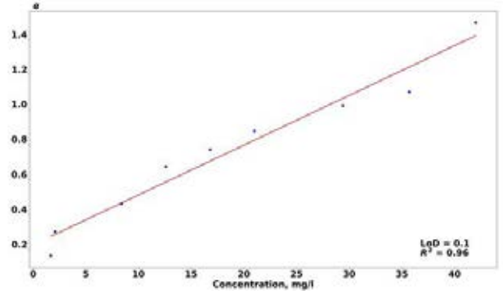

Figure 10. The calibration function for the DMA solution by α as the integral parameter.

The LIF spectrum was received with a daylight background (Figure 11). This spectrum was received by the LIF sensor at 1 m of height above the surface of the solution (the setup is in Figure 1).

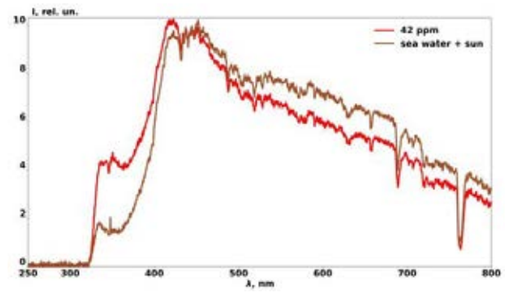

Figure 11. LIF spectrum of the DMA with a daylight background by LIDAR sounding.

Slick spectra of 300 ,100 ,20 and 500 μm thickness were measured, and the example of such distribution is shown in Figure 13. Different colors in the upper part correspond to the different types of slicks.

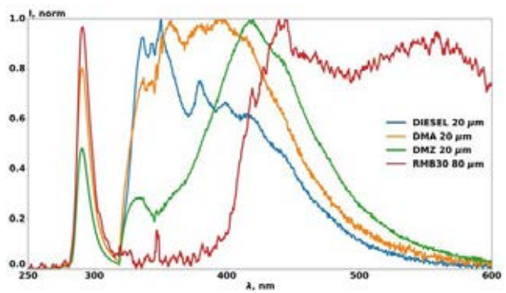

Figure 13. LIF slick spectra of the different types of oil products.

Experimental results showed that the shapes of LIF spectra changed significantly depending on the state of the oil product. The spectral distribution of the LIF for the same oil products was quite different and depended on the state (pure state, slick or solution). The dissolved fraction caused a fairly narrow maximum in the spectra of the oil products and this maximum was displaced to the shortwave band. The spectra of the oil product slicks are the intermediate stage of the spectrum between the pure fuel and the solution. This phenomenon should be concerned when the LIF method was used to identify the types of oil products in the bilge water or the slick on the sea surface. It is necessary to have etalons of the LIF spectra of oil products in the relevant state in which it can be found in the oil pollution (slick or solution state). The shape of the solution lines has the maximum within the band of 370-330 nm, and the full width at half maximum is about 70–40 nm. The spectra with a distinctive shape of each type may be used as specific characteristics for the recognition by machine learning. Heavy types of fuel have typical tails of the spectral distribution within the wavelength band of 550–400 nm. Narrow lines of absorption were observed in the LIF spectrum within a 360-320 nm band. There could be several absorption lines for the heavy types. The absorption feature of the LIF of the solutions of the researched oil products at the 346 nm was distinctive. This therefore indicates that if there is a dissolved fraction of oil product, it may be used to measure concentrations of oil products in the solution as well as the integral α parameter of the fluorescence spectra. It may be useful if there are different types of oil products in the bilge water.

Experiments showed that the shape of the LIF spectra from solutions and fluorescence intensity changed as time passed. It may be caused by the diverse weathering processes of oil hydrocarbons. It is not easy to simulate natural weathering conditions of the sea at the laboratory. The samples were prepared and investigated, so that the influence of the dissolution on the complexes would be leading the process. This makes the shape of the LIF spectrum change or it reduces the quantum efficiency of the fluorescence since the research was aimed to improve the LIF for the recognition of oil product solutions.

Dynamic research of the LIF spectra from the solutions shows that the shape of the LIF spectra was not significantly changed if the weathering was minimized. Nonetheless, the efficiency of LIF reduces significantly (more than two times in five days). More significant changes in the LIF efficiency were caused by photochemical weathering and vaporization. The appearance of the spectral component in the shortwave range from the main maximum and the reduction of the fluorescence signal was observed. It should be concerned when the concentration of oil products was measured. In addition, such dynamics of the LIF spectra should be of concern when methods of machine learning for fuel type identification by LIF spectra are being developed. It is essential to develop a dynamic matrix of features for each type of fuel. The procedure of machine learning should include either the identification of fuel type or the time when the oil product enters the seawater.

The spectra of the LIF slicks from the oil products were researched in many works. In this research, the investigation of the LIF spectra was aimed to be used for machine learning (data sets collection of the researched types of fuel) and to define the distinctive features of the LIF spectra in the time of excitation by UV radiation. The spectral features of LIF from the slicks of light fuels only were studied. The band of the slick thickness from 20 μm to 500 μm was studied. The main results obtained agreed with the results in:

- The LIF spectra almost agreed for the different thicknesses of the slicks of the same type of fuel. For now, it is not possible to receive information about the slick thickness from LIF spectra. It is crucial to find new solutions for LIF application to receive this information;
- The study of slick dynamics from the light type of fuels showed that the spectral distribution form of the LIF spectra of thin slick (300–20 μm) does not change much.

The study of the LIF spectra from the slicks of heavy types of fuel was complicated, and it was not managed to receive great statistics of measurements for different thicknesses. It was caused by a robust heterogeneous thickness of the slick surface. As a result, the LIF spectra were a sum of all the spectral distributions from different thicknesses. Thus, the spectral features of some slicks and thicknesses were being smoothed. This factor will be more crucial at sea because there will be many environmental influences on the slick and it will cause the rise of the slick thickness range. It is essential to provide additional in situ measurements.

The results of the light types of fuels may be already used in machine learning for the oil product identification of slicks by the LIF. The spectral distribution of LIF features is specific for the investigated types of oil products. Concerning heavy types of marine fuel, additional in situ research is essential to investigate how thickness and its distribution in the slick are spread under the environmental influence. It is crucial to provide numerous measurements and collect data sets of LIF spectra features for machine learning to identify heavy types of fuel. Today, the quantity of such data sets is lacking. The small-sized LIF sensor is being tested for UAV to collect a comparative data set in situ. The advantages of using UV radiation are as follows: the ability to monitor slicks and dissolved oil hydrocarbons at daylight; the high values of the quantum efficiency of LIF if UV radiation is used.

The disadvantages are as follows: heights are low due to the absorption of the atmosphere and LIF spectra are obtained from the very surface of the seawater (due to the strong absorption in the seawater); this is not crucial for the slicks, but this could be important for the solutions.

The values of the solution concentration in the upper layer of the ocean and under the surface may vary quite significantly. It is essential to provide measurement in the on-land regime and under the surface.

Conclusions:

The LIF spectra dependence on oil product type and state is complicated. The form of LIF spectral distribution changes as time progresses. Nonetheless, still the research of these dependencies allows using this method to identify features of different types of marine fuel which are dissolved in the seawater or are promptly in the slick.

The identification and measurement of dissolved oil products in the seawater are the strong potential of using this method. This method can be well used to control such a giant source of ocean pollution as bilge water disposal by vessels, especially concerning the low values of LoD. Monitoring methods that are based on the LIF spectroscopy may be used to identify the oil products that built up the slick. It is necessary to provide further research so that it will be possible to determine the dependence of LIF spectra parameters on slick thickness. It is quite perspective to use UAV for either regional-scale monitoring or collecting LIF spectra data sets. It will be used to provide machine learning for the identification of oil product type and the measurement of pollution volume as a solution state and slick.

Reference:

O. Bukin, D. Proschenko, C. Alexey et al., Photonics, vol. 7, no. 2, pp. 36, 2020.

Mitra Amoli Diva
PhD in Analytical Chemistry
Spectroscopy Application Manager

Real-Time Thickness Measurement of Marine Oil Spill by Fiber-Optic Surface Plasmon Resonance Sensors

Oil Spills have emerged as a major threat to marine ecosystems in recent years, arousing considerable political, environmental, and scientific concern. The large-scale industrial disaster caused by the explosion of the Deepwater Horizon platform of British Petroleum in the Gulf of Mexico resulted in an estimated -200million-gallon oil spill. Then, severe air contamination was caused by approximately 2 million gallons of dispersant chemicals that were applied to clean the spill. The disaster resulted in adverse health effects and significant damage to the gulf ecosystem. Oil spills are harmful to large areas, including numerous habitats, species, and ecological functions. Offshore oil spills share the characteristics of rapid onset, large distribution, and high drift and dispersion dynamics.

Due to such broad negative consequences, achieving rapid oil spill emergency response and hazard assessment of ocean oil spills are of great significance. Oil slick thickness measurement is directly related to the estimation of oil leak scale and selecting and optimizing oil spill countermeasures. The detection of slick thickness is also useful to determine the effectiveness of such countermeasures (e.g., in situ burning and chemical dispersion) and understand the physical distribution of oil in the sea and its spreading rates. Although at an early stage of development, achieving accurate measurement of oil thickness is critical, especially for real-time detection. Some oil thickness measurement methods have been developed, both in the laboratory and in the field, employing concepts that include near-infrared reflectance, spectral differences, infrared emission, and radar methods-wave damping. To date, various sensing technologies have been applied in the measurement of oil slicks on the sea surface and include optical (visible and infrared multispectral and hyperspectral), microwave [synthetic aperture radar (SAR)], side-looking airborne radar (SLAR), microwave radiometer, laser fluorescence, and thermal sensors. Garcia-Pineda et al. (2020) summarized the methods used for the rapid classification of oil types and thickness estimation. Among these, SAR was determined as suitable for large areas and long-distance monitoring at night and in bad weather, with good spatial resolution. Oil spills appear dark in SAR images because sea surface capillaries and short gravity waves can be dampened by oil. However, the phenomenon of dark areas in SAR images is difficult to clarify as they can also be caused by natural surface films produced by plankton or fish, grease, floating algae, and internal waves. Laser fluorescence sensors also have all-weather characteristics and distinguish oil from other substances by its strong fluorescence characteristics. Thermal sensors can detect oil by thermal comparisons generated by the different emissivity of water

and oil on the sea surface, which can also indicate its thickness. Optical sensors have been successfully used to detect the presence of oil and quantify its volume or thickness. In terms of spectral differences, several studies have reported the correlation between slick thickness and specific wavelengths ranging over the visible spectrum. However, researchers have reported different changes in spectral brightness or reflectance as a result of increased thickness and reached contradictory conclusion.

Several fiber-optic sensor structures based on surface plasmon resonance (SPR) have been reported as follows: hetero-core, U-shaped, D-shaped, tapered, end-face reflected, and unclad/etched sensing structures. Unclad/etched sensing structures are made by removing the part of the optical fiber cladding and then coating the sensing region on the fiber surface with metal film (using silver, gold, platinum, and other metals) via physical evaporation, sputtering, or electroless plating (ELP). ELP is a chemical coating technique based on the chemical reduction of metal ions, which in turn deposits metals on the surface of the substrate. ELP is beneficial in the preparation of fiber-optic SPR sensors as it can overcome physical evaporation or sputtering difficulties when forming uniform films on very thin fiber-optic cylinders.

This paper introduced a novel real-time technique to measure oil slick thickness rapidly and effectively using a gold-film fiber-optic surface plasmon resonance (FOSPR) sensor in this study (Figure 1). The sensor is prepared using PDA accelerated wet chemical plating. While most detection methods can measure the thickness of oil on seawater, they fail to detect submarine oil leakages. The terminal reflective FOSPR sensors proposed in this study can achieve detection in the flow cell and immersion situations and eliminate electromagnetic interference in seawater detection. The spectral reflectance reduces as the thickness of the oil slick increases, making it possible to use FOSPR sensors to determine oil slick thickness. the effects of salinity and temperature on oil thickness measurement was examined in detail and investigated the repeatability of the sensors. Rapid detection of oil spills and measurement of oil slicks using FOSPR sensors are expected to provide timely marine pollution prevention to minimize the threat to marine ecosystems.

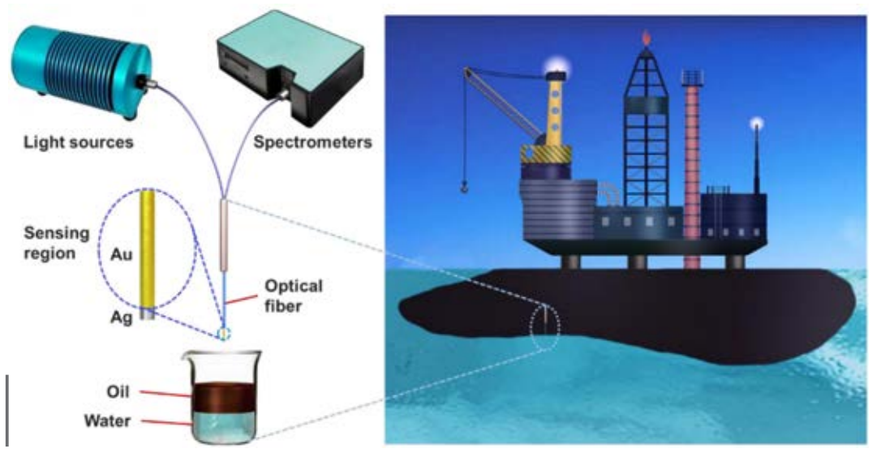

Figure 1. Schematic diagram of oil slick thickness measurements by fiber-optic surface plasmon resonance (FOSPR) sensor.

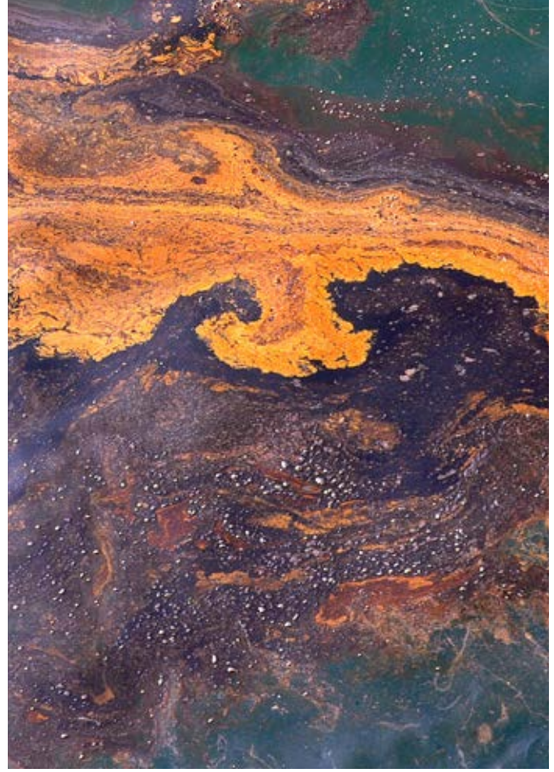

Fabrication of the Fiber-Optic Surface Plasmon Resonance Sensor:

The cladding was stripped at one end of the multimode optical fiber using chemical methods to expose the fiber core. Then, the end face of the fiber core was polished. A photograph of the FOSPR sensor for oil detection is presented in Figure 2. PDA coating is a universal material for optical fiber functionalization by dopamine self-polymerization. In this study, the gold-film fiber sensor was fabricated by PDA-accelerated ELP, which was reported in our previous study. In brief, the piranha solution was employed to clean the bare fiber for 30 min at °90C, and then, the cleaned optical fiber was immersed in a dopamine solution at °10C for 15 min. The PDA functionalized fiber adsorbed the gold seeds via immersion in colloidal gold solution for 2 h, which was synthesized by sodium citrate, NaBH4, and gold (III) chloride trihydrate. Finally, the gold film was generated on the optical fiber by immersing the gold seed fiber in a solution with a mixture of 0.1 wt% gold (III) chloride trihydrate and 0.4 mM hydroxylamine hydrochloride and shaking for 5 min 30 s. The thin silver layer was coated onto the end surface of the gold film-coated fiber by a silver mirror reaction using Tollens' reagent. The resulting silver mirror is an essential component of the FOSPR sensor, which is responsible for the back reflection of the light in the fiber.

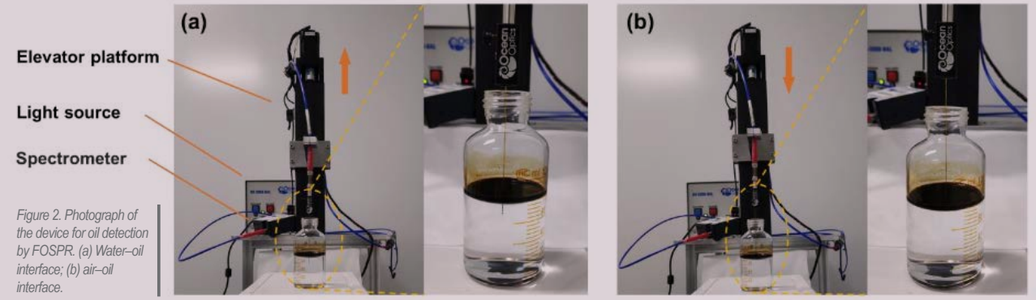

Figure 2. Photograph of the device for oil detection by FOSPR. (a) Water–oil interface; (b) air–oil interface.

Fiber-Optic Surface Plasmon Resonance Sensor Set Up:

A diagram of the sensor measurement system is shown in Figure 1 and Figure 2. A tungsten-halogen light source (DH--2000BAL, Ocean Optics, Inc.) was used to provide stable UV-visible light at wavelengths between 200 and 1,000 nm. In this study, a 1,000–360 nm halogen light was employed, which entered the FOSPR sensor through a Y-type optical fiber (SPLIT-400-VIS-NIR, Ocean Optics, Inc.). The sensing-region end of the FOSPR sensor was immersed in the solution to be measured. After SPR occurred under the excitation of the incident light, the signal was transmitted to the spectrometer (USB+2000, Ocean Optics, Inc.) through the other side of the Y-type optical fiber. The signal was displayed and monitored by a computer connected to the spectrometer. The thickness of the light crude oil film was detected using the fabricated FOSPR sensor, and the linear relationship between the intensity and thickness of the light crude oil film was calculated.

Detection of Oil Spill:

As illustrated in Figure 1, the proposed FOSPR sensors can be set up near the oil spill point in the sea. Significant changes in light intensity and resonance wavelength can be observed, which arise from the differences in refraction between oil and water/air. Research has demonstrated that spectral differences can be used to research the relationship between thickness and specific wavelengths, where wavelengths in the visible and near-infrared range are related to the oil slick thickness. A wavelength range of 1,000–500 nm was employed to study the reflectance change of oil slick thickness in the wavelength range. It was also found that different oil thicknesses led to changes in reflection spectra.

Oil slick thickness was examined at the water-oil, air-oil, and air-liquid interfaces, respectively (Figure 2). Then, the thickness measurement of crude oil was carried out, in which crude oil with different volumes was added to the water surface. A pipette was used to accurately measure the volume of crude oil and calculated the thickness h of oil from the volume of crude oil on container S (the bottom area of the container used was 20 cm2):

$$h=V/Sh=V/S$$

The total length of the sensing region was 10 mm, where the silver end was placed at the bottom of the sensor to enhance reflection. According to Supplementary Figure 1, an elevator platform was used to precisely control the height of the sensor. The sensing region was completely immersed in water at the water-oil interface. It was necessary to add a certain amount of oil and raise the fiber-optic sensor upward to keep the top of the sensor on the water-oil interface. The sensing region was exposed to the air while the silver end of the sensor was in the water at the air-oil interface. Thickness estimation at the water-oil and air-oil interfaces was carried out by adding a certain amount of oil to reach a thickness ranging from 0 to 10 mm. At the air-water interface, half of the sensing region was immersed in water, and the other was in the air to determine the minimum thickness that our SPR sensor could measure. The effects of temperature and salinity, which are common factors in oil thickness monitoring was also investigated on the FOSPR sensor response.

Principles of Oil Detection:

Surface plasmon resonance occurs at the sensing region covered with a metal nanofilm when white light is continuously conducted with total reflection in the optical fiber and transmitted from one end to the optical fiber sensing region. As the refractive index changes in the surrounding environment arising from oil spillage, the SPR spectra also change, and the entire sensing region of the FOSPR sensor provides a detection function. The measurement of oil thickness is implemented by detecting the interfaces between different liquid layers (air-oil and oil-water).

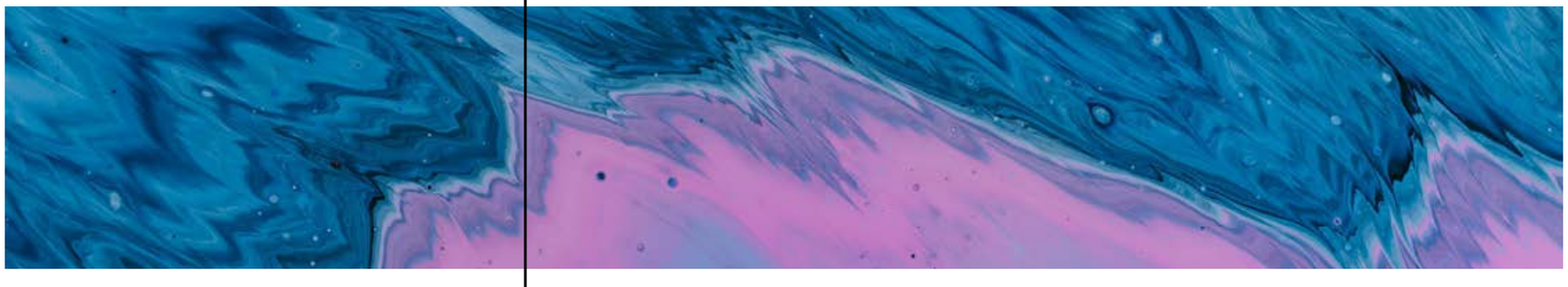

Measurement of Oil Slick Thickness:

Thickness estimation at the water-oil interface was carried out by adding oil to reach a thickness ranging from 0 to 10 mm. While adding a certain amount of petroleum, the FOSPR sensor was raised upward to keep it at the top of the sensing region at the air-oil interface (Figure 3A). As shown in Figure 3B, the reflectance of oil declines at the oil-water interface as visible thickness increases from 500 to 1,000 nm, which is in line with previous research on the spectral responses of offshore oil slicks (Lu et al., 2013 ,2008). Based on the reflection spectrum corresponding to the wavelength of 682.91 nm, the oil slick thickness is linearly fitted to obtain a linear relationship with a measurement coefficient R2 of 0.955, as shown in Figure 3C.

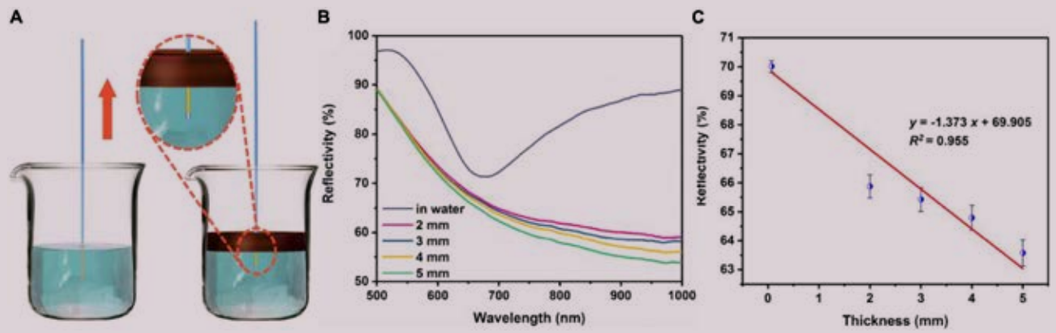

Figure 3. (A) Schematic diagram of oil detection at the water-oil interface by FOSPR sensor (the top of the sensing region is kept on top of the oil); (B) Reflectivity spectra of the electroless-plated optical fiber surface plasmon resonance (SPR) sensors in the water-oil interface with different oil spill thicknesses; and (C) Linear curve of reflectivity and oil slick thickness (the linear relationship is based on a wavelength of 682.91 nm).

Thickness detection at the air-oil interface was carried out by adding oil to reach a thickness range of 5-0 mm. As illustrated in Figure 4A, at the air-oil interface, the silver end is immersed in the water, and the sensing region remains in the air. The optical fiber sensor is used to measure the oil slick thickness in the air. Figure 4B shows that the reflectance spectrum gradually decreases as the oil slick thickness increases, and the coefficient R2 is 0.998. High correlations are observed between oil spill spectral reflectance values and oil spill thickness measurements. The thick oil slick is characterized by low reflection, low penetrability, and strong absorption of incident visible light.

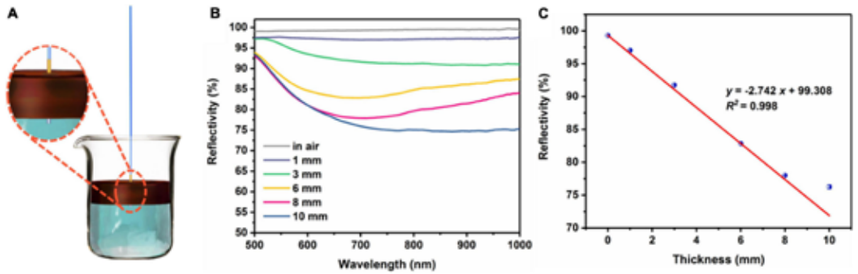

Figure 4. (A) Schematic diagram of oil detection at the air-oil interface by FOSPR sensor (the bottom of sensing region remains at the bottom of the oil); (B) Reflectivity spectra of the electroless-plated optical fiber SPR sensors in air-oil interface with different oil spill thicknesses; and (C) Linear curve of reflectivity and height (this linear relationship is based on a wavelength of 700.6 nm).

Effects of Salinity and Temperature:

Different salinities (%45–25) were used to determine the influence of ocean salinity fluctuations on oil thickness estimation according to the average salinity of the seawater, which was %35. The temperature range of water and oil was °40–20C. As illustrated in Figure 5, the spectrogram does not change significantly as the salinity and temperature increase. This indicates that changes in salinity and temperature (whether water or oil) have less effect on the measurement of oil slick thickness by the proposed sensor.

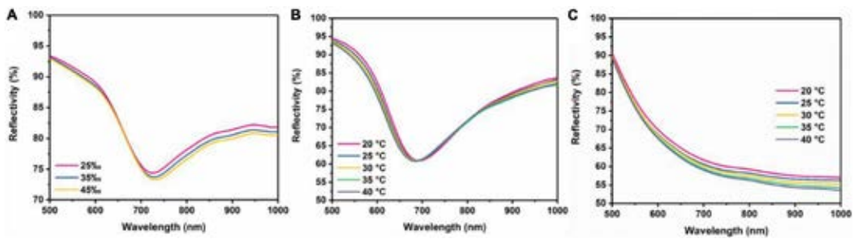

Figure 5. Reflectivity spectra of the FOSPR sensor in water with different (A) salinities and (B) temperatures and (C) reflectivity spectra of the FOSPR sensor in oil with different temperatures.

Repeatability:

To explore the reusability of the optical fiber sensor after oil thickness measurement, the used FOSPR sensor was cleaned with water and detergent, followed by ozone treatment. In detail, the sensing regions of optical fiber were soaked in ultrapure water filled with detergent for approximately 10 min and then treated by ozone for 2 h (Figure 6A). As shown in Figure 6B, the spectrum of the sensor after cleaning returns to the resonance wavelength position before oil detection at a certain degree.

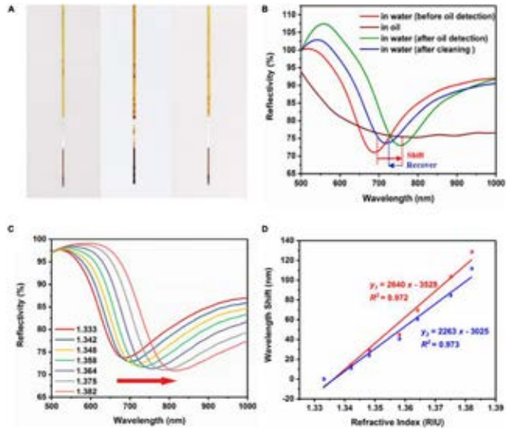

Figure 6. Sensor repeatability experiment: (A) Photograph of optical SPR sensors (from left to right: initial, after oil detection, and after cleaning); (B) Optical SPR sensor spectrum under different processing; (C) Reflectivity spectra of the sensor in glucose solution with varying refractive indices; and (D) Linear curve of the wavelength shift and concentration of glucose solution (y1: the sensitivity of optical SPR sensors before detecting oil, and y2: the sensitivity of optical SPR sensors after cleaning).

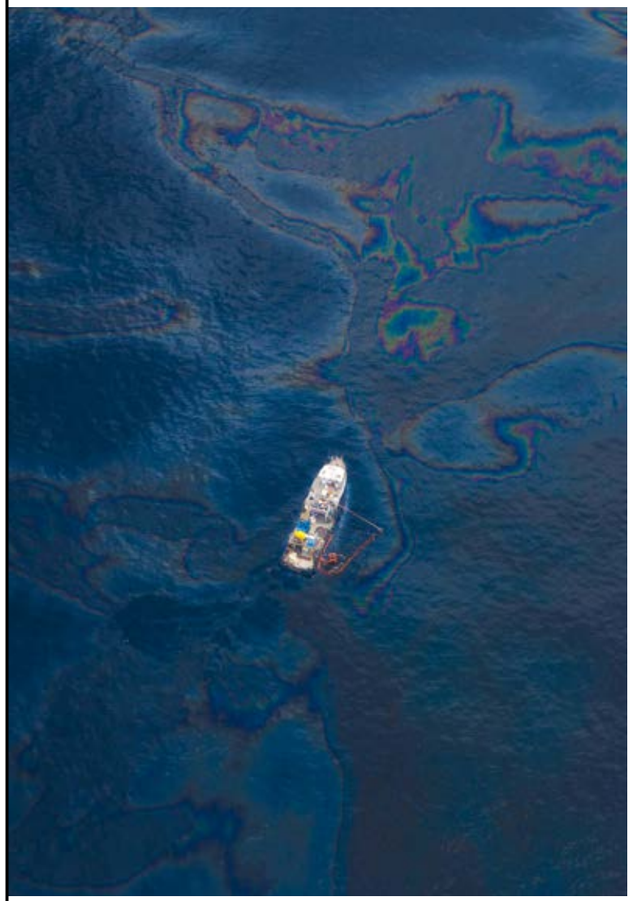

To determine the sensitivity of the as-cleaned sensor to the surrounding refractive index, the sensor was immersed in a series of different mass concentrations of sucrose solutions of varying refractive indices, ranging from 1.33 to 1.40. Then, a comparison experiment was conducted by immersing the optical fiber SPR sensor and cleaning sensor into the different concentrations of glucose solution. As shown in Figure 6C, the SPR wavelength redshifts with an increase in the refractive index. The blue line in Figure 6D indicates that the sensitivity of the cleaning sensor is 2,263 nm/RIU, which is lower than the red line, which has a sensitivity of 2,640 nm/RIU. The results show that the sensor after exposure to petroleum can still be used for detection, with a slight decrease in the sensitivity.

Discussion:

The thickness of oil is usually correlated to its visual appearance and color. Several measurement methods, such as microwave radiometry, laser fluorescence, and thermal sensors, have been applied to detect oil spills, and their advantages and disadvantages were summarized in Table 1. Among these, microwave sensors have been used for a long time as indicators of oil slick thickness as the microwave brightness of slicks varies in a cyclical fashion with the thickness. Unfortunately, microwave brightness is also influenced by a number of other factors, such as weather, sea conditions, and the type of oil. Comparatively, fabricated fiber-optic SPR sensors show significant promise for detecting oil thickness, with real-time capabilities, high flexibility, corrosion resistance, and low cost. The high salt concentration in most marine environments combined with

high electrical conductivity makes marine bodies a highly conducive environment for corrosion to occur on metal surfaces, including iron and zinc. However, as the optical fiber SPR sensor is made of glass and has a gold layer with corrosion resistance, it does not encounter this problem.

This paper simulated two situations of offshore oil spills in this study. The FOSPR sensor was immersed in water or oil and detected at two interfaces (water-oil and air-oil). In the construction of the entire optical fiber detection system, a fishing float was employed to ensure that the sensing area of the optical fiber sensor was perpendicular to the sea surface. The sensor responded quickly when oil drops appeared on the surface, and the sensing signal was transmitted to a computer and reflected by changes in light intensity and resonance wavelength. The measurement sensitivity of oil thickness at the air-oil interface was higher than at the water-oil interface, which could be due to the greater refractive index difference between air and oil compared with that of water and oil.

As displayed in Figures 3, and 4, it can be seen that the sensor responded effectively when it came into contact with oil. A linear curve of reflectivity and oil slick thickness was obtained using a fixed wavelength. The linear relationships were based on a wavelength of 682.91 nm for water-oil and a wavelength of 700.6 nm for air-oil, respectively. The reflectance corresponding to the wavelength of 700.6 nm at the air-oil interface could be determined from the detection reflection spectrogram of the spilled oil. Thus, oil thickness in different conditions could be calculated based on the relationship curve between thickness and reflectivity.

Measurement methods	Principle	Advantage	Disadvantage	MDT[a]	References
Microwave radiometry	Brightness variation	Good spatial resolution; extensive application	Disturbed by external factors; expensive	/	(Garcia-Pineda et al., 2020)
Laser fluorescence	Fluorescence intensity	All-weather characteristics	Only for thin oil film	/	(Cui et al., 2021)
Thermal sensors	Thermal comparisons	Thermal imaging detection	Photo-oxidation, biodegradation	40 μm at noon, 150 μm at midnight	(Lu et al., 2016)
FOSPR sensor	Reflection intensity	Real-time, high flexibility, corrosion resistance, and anti-interference; can be used under-water detection	/	70 μm	This work

[a] MDT = minimum detectable thickness

Table 1: Comparison of oil film thickness measurement methods.

Conclusion:

This paper was proposed an optical fiber SPR sensor for the rapid measurement of oil slick thickness in this study. Two oil thickness measurement methods under different interfaces were presented. The measurement results at the water-oil interface showed that the sensor had a high sensitivity of %1.373−/mm in the thickness range of 5–0 mm; at the air-oil interface, the sensor presented a sensitivity of %2.742−/mm in the thickness range of 10–0 mm. Experimental results also indicated that salinity and temperature changes had less influence on oil thickness measurement, and the FOSPR sensor had good repeatability. The unique advantages of optical fiber have significant application prospects for use in marine oil spill detection and thickness measurements, such as miniaturization, high flexibility, corrosion resistance, and anti-interference. The proposed FOSPR sensor has great potential for submarine oil spill detection at the water-oil interface.

Reference:

H. Yin, S. Chen, R. Huang et al., Frontiers in Marine Science, vol. 8, 2022-January-06, 2022.

Houshang Noorizadeh
PhD in Analytical Chemistry
Chromatography Product Manager

Simultaneously Determination of Oxyhalides

(Bromate & Chlorate) in Presence of Common Inorganic Anions with ion Chromatography in Drinking water

Introduction:

In Drinking disinfection eliminate or remove the pathogens that are responsible for waterborne diseases. There are many ways for disinfection water supplies such as ozonation and chlorination in water treatment process. Oxyhalide specially bromate is identified as by-product of disinfection of drinking water which is cause many health problems such as cancer. So determination of their concentration level is very important. Also monitoring of common inorganic anions concentration is necessary.

This application note trying to introduce method for simultaneously determination of Fluoride, chlorite, Bromate, Chloride, Nitrite, Bromide,

Chlorate, Nitrate, Phosphate and Sulfate in drinking water using anion chromatography with suppressed conductivity detection. This method can analyze common inorganic anions and oxyhalides simultaneously with high resolution. Dichloroacetate (DCA-) as a surrogate substance is also well separated. Water dip and carbonate system peak do not overlap with other peaks.

Instrumentation and experimental:

Ion chromatography system (S1130 high pressure IC pump, S5300 autosampler, S150 Conductivity detector, column oven and suppressor) from Sykam, IC SI4 52-E anionic column from Shodex is used.

Instrument is run with 3.6 mM Na2CO3 as mobile phase. After equilibration (reach the temperature to 45 ˚C and flow rate to 0.8 ml/min), 50 µL filtered water sample is injected to instrument by autosampler. The results (figure 1) shows high resolution in anions separation.

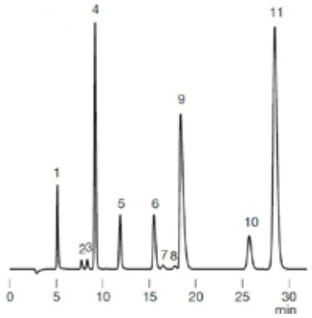

Figure 1. determination of common inorganic anions and oxyhalids

Also table 1 demonstrate the concentration of anions calibration levels. Because of difference concentration level of anions on drinking water, the standard calibration concentrations are from ppb to ppb and different form each anion.

Peak number	Component	Concentration level 1 (ppm)	Concentration level 2 (ppm)	Concentration level 3 (ppm)	Concentration level 4 (ppm)
1	Fluoride	0.05	0.25	0.5	1
2	chlorite	0.005	0.025	0.05	0.1
3	Bromate	0.005	0.025	0.05	0.1
4	Chloride	5	25	50	100
5	Nitrite	0.05	0.25	0.5	1
6	Bromide	0.05	0.25	0.5	1
7	Chlorate	0.005	0.025	0.05	0.1
8	Dichloroacetate	0.05	0.25	0.5	1
9	Nitrate	2	10	20	40
10	Phosphate	0.05	0.25	0.5	1
11	Sulfate	5	25	50	100

Table 1: concentration levels of standard samples

Calibration curve for each anion is plotted and samples concentration is computed. Concentration of anions in tested drinking water represent in table 2.

Table 2: concentration of typical drinking water

Component	Concentration (ppm)
Fluoride	0.632
chlorite	0.112
Bromate	0.002
Chloride	35
Nitrite	NA
Bromide	0.063
Chlorate	0.235
Dichloroacetate	NA
Nitrate	5.312
Phosphate	0.042
Sulfate	42

Reference:

[1] EPA method 300: determination of inorganic anions by ion chromatography, Rev. 1993 ,2.1
[2] EPA method 300.1: determination of inorganic anions in drinking water by ion chromatography, Rev. 1997 ,1.0
[3] www.Sykam.com
[4] www.Shodex.com

Farid Sheikh-Hasani
MSc of polymer chemistry
Particle & Polymer Testing Product Manager

Comminution of Plastic PET Bottles

Packaging Regulations Mandate the Processing:

PET Can be recycled thanks to a wide variety of methods: mechanical, melt reprocessing, molecule break down (de-polymerisation), purification and re-polymerisation as well as energy recovery. In the past, a lot of plastic was favored in the steel and cement industry as a source of energy. With the rise of crude oil prices became - besides the thermal use - also the adaptation to new packaging materials economically interesting. Prerequisite for this is the at least the reasonably genuine provision of the plastic materials. For this purpose, the return of the PET bottles by the consumers is an obvious solution.

Processing of Used PET Bottles:

The waste manager is now having the task of processing these materials. For this purpose, the plastic bottles are shredded. This process creates pieces (so called flecks) of an average size of 3 x 12 mm and also naturally a very fine dust. With a suitable cleaning process, the shredded product is washed absolutely clean. The separation from other plastics, like for example PP (polypropylene) or PE (polyethylene) from which mostly the screw caps are made, is accomplished with the sink and float method with a density separation. After the drying, the paper labels may also be removed with a blowing off process. The flecks are sold in this state by the recycling firms. For further processing, the fine share must be extruded and the resulting granulate is then also sold.

A Broad Analytical Evaluation is Mandatoty:

The production of higher quality products from this recycled material requires a broad analytical evaluation. For this purpose, a comminution of the flecks as well as the granules is necessary. The parameters to be evaluated are among others factors, the degree of polymerization and the color. A statement about the degree of polymerization and thus on mechanical or thermal damage is obtained via the determination of the melt-index. This determination is a wide spread method in the field of chemical polymers. The measured value depends on the particle size. The color is determined via white level measurement. But the measured data is greatly dependent on the reflected light and therewith also on the particle size. Therefore prior to the determination of the melt-index and before the measurement of the white level, the samples always must be prepared in a reproducible manner.

The FRITSCH Variable Speed Rotor Mill PULVERISETTE 14 classic line is the ideal mill for fast, effective comminution of soft to medium-hard, brittle and fibrous materials as well as temperature-sensitive samples – proven worldwide for the use in trace analysis. The ingenious air routing of the PULVERISETTE 14 classic line ensures a constant airflow to cool the rotor, all motor components and the grinding material in the collecting vessel.

Difficult-to-mill samples, or extremely temperature-sensitive samples such as styrenes, polyester, synthetic resins, films, PVC, PP and PE can be embrittled with the addition of liquid nitrogen and afterwards ground in the PULVERISETTE 14. Utilized for the defined preparation of the samples is the Variable Speed Rotor Mill PULVERISETTE 14 classic line, inclusive the impact rotor with 12 ribs and a sieve with 1 mm mesh width. The rotational speed control for the cutting rotor is for the achievement of the reproducible results immensely important. Frequently for polyethylene terephthalate we recommend to work with 16,000 rpm. Tests by the users in this concrete case led to the settings of lower rotational speeds. Dependent on products and testing parameters, the optimum rotational speed was set between 10,000 and 14,000 rpm. These low rotational speeds of the rotors minimize the mechanical, respectively the thermal demands during the comminution. Consequently, a lower throughput is to be expected. Alternatively, could the material be embrittled and added at higher rotational speeds.

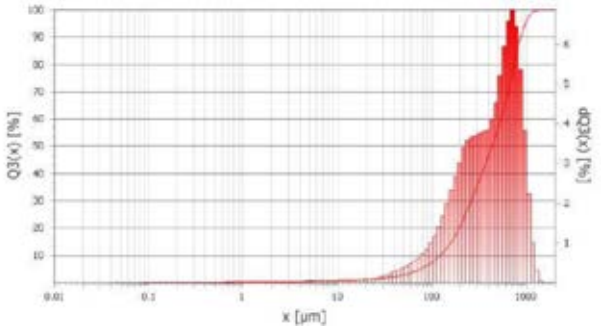

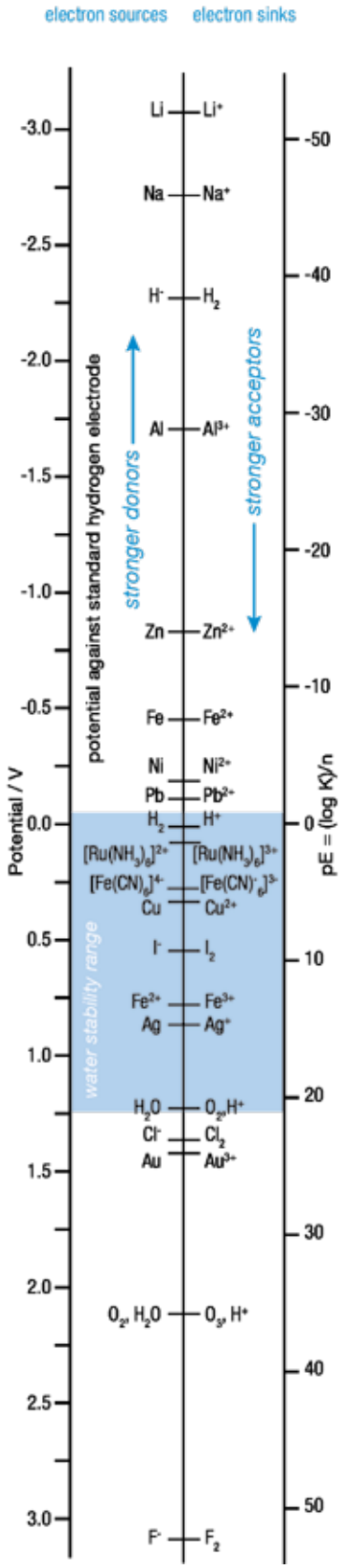

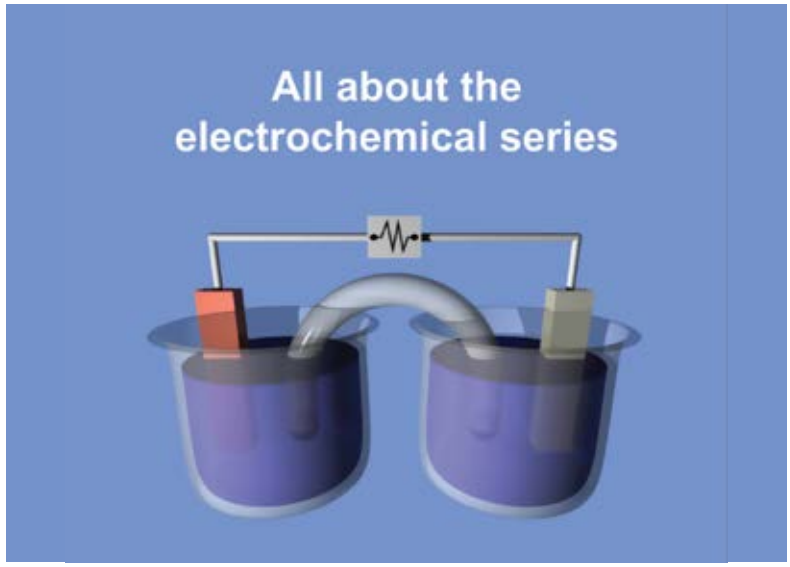

Nernst equation:	$E = E^0 + \frac{R \cdot T}{z \cdot F} \cdot \ln \frac{c(Ox)}{c(Red)}$
For a cell at 25 °C:	$E = E^0 + \frac{0{,}05916V}{z} \cdot \log_{10} \frac{c(Ox)}{c(Red)}$
Faraday's law:	$m = \frac{M \cdot Q}{z \cdot F}$

elementary charge	$e = 1.60217662 \cdot 10^{-19}\ C$
Avogadro constant	$N_A = 6.0221409 \cdot 10^{23}\ mol^{-1}$
gas constant	$R = N_A k_B$ $8.31446\ Jmol^{-1}\ K^{-1}$
molar volume	$V_m = 22.41383\ L/mol$ (0 °C, 1 atm)
Faraday constant	$F = eN_A$ $9.64853 \cdot 10^4\ C/mol$


ARA
INFORMATION